

Electrochemical Corrosion of Pb-Sn and Pb-Sb Alloys for Lead-Acid Battery Applications

Z. BAKOUR* AND A. DAKHOUCHE

Laboratory of Inorganic Materials, Faculty of Sciences, University Mohamed Boudiaf of M'sila, 28000 M'sila, Algeria

The aim of this study was to compare the electrochemical corrosion behavior of as-cast Pb-Sn and Pb-Sb alloy samples in the 0.5 M H₂SO₄ solution at 25 °C. Electrochemical impedance spectroscopy (EIS) diagrams, potentiodynamic polarization curves and the equivalent circuit analysis were used to evaluate the electrochemical corrosion response. It was found that Pb-1 wt.% Sn alloy exhibits a microstructure with large cellular array and better electrochemical corrosion resistance than that of Pb-1 wt.% Sb.

DOI: [10.12693/APhysPolA.134.103](https://doi.org/10.12693/APhysPolA.134.103)

PACS/topics: corrosion, lead-acid battery, microstructure, alloys

1. Introduction

Pb-Sn, Pb-Sb and Pb-Ca-Sn alloys are commonly used in the production of positive and negative grids, of both the valve-regulated lead-acid (VRLA) and the starting, lighting and ignition (SLI) batteries [1, 2]. It is well known that the use of Sb (e.g. at positive SLI battery grids) enhances electrolysis of water into hydrogen and oxygen during charging, leading to water or electrolyte loss. According to [3–5], Pb-Sn and Pb-Sn(Ca) alloys appear to be a good alternative for decreasing water decomposition. It was reported [1] that Pb-Sb alloys corrode more rapidly than Pb-Sn.

2. Experimental procedure

Pb-1 wt.% Sn and Pb-1 wt.% Sb binary alloys were prepared using commercially pure metals: Pb (99.89 wt.%), Sn (99.99 wt.%) and Sb (99.33 wt.%). The alloys were melted in a crucible at 350 °C and 600 °C, respectively in an electrical furnace for 30 min, and maintained under these conditions for 1 h to form a homogeneous Pb-1 wt.% Sn and Pb-1 wt.% Sb alloys. These alloys were cast into a cylindrical mold with diameter of 15 mm and length of 10 mm. The cooling for both alloys was carried out in air.

As-cast specimens were sectioned through the center of the ingot, ground, polished and etched to reveal the macrostructure. A mixture of citric acid and ammonium molybdate 250 and 100 g, respectively, for 1 l of water was used as the etchant.

The samples were polished and etched by using 37 cm³ of glacial acetic acid and 15 cm³ of H₂O₂ solution at room temperature for microscopy examination. The microstructural characterization was carried out by using an optical microscope associated with an image processing system (A59.2207 digital camera of eyepiece type).

In order to evaluate the electrochemical corrosion behavior of the Pb-1 wt.% Sn and Pb-1 wt.% Sb alloys, electrochemical corrosion tests were performed on a 1.32 cm² circular area.

The surface of the lead electrode was mechanically polished with 800, 1500 and 2000 grade SiC emery paper.

Electrochemical impedance spectroscopy (EIS) measurements began after an initial delay of 35 min, which was needed for the samples to reach a steady-state condition. The tests were carried out with the samples immersed in 250 cm³ of a stagnant and naturally aerated 0.5 M H₂SO₄ solution at 25 °C. A potentiostat/galvanostat (Voltalab[®] PGZ 402) controlled by VoltaMaster 4 software, a glass corrosion cell kit with a pure Pb counter-electrode and a Hg/Hg₂SO₄/K₂SO₄ saturated reference electrode (MSE) were used to perform the EIS tests. The potential amplitude was set to 10 mV peak-to-peak (AC signal), with ten points per decade. The frequency range was set from 100 mHz to 100 kHz.

Potentiodynamic measurements were also carried out in the aforementioned solution at 25 °C using the same potentiostat. These tests were performed by stepping the potential at a scan rate of 10 mVs⁻¹ from -1200 mV (MSE) to 1200 mV (MSE). Tafel plots using both anodic and cathodic branches at a scan rate of 10 mVs⁻¹ from -1200 mV (MSE) to +0 mV (MSE) were plotted using potentiodynamic polarization curves. In order to give quantitative support to our discussion of these experimental EIS results, an appropriate model (ZView version 2) for equivalent circuit quantification was used.

3. Results and discussion

3.1. Microstructure of alloys

Optical micrographs of the Pb-1 wt.% Sn and Pb-1 wt.% Sb alloys, are shown in Fig. 1a and b, respectively. The morphology structure of Pb-1 wt.% Sn and Pb-1 wt.% Sb alloys obtained using given cooling rate is similar. Both alloys contain large-size grains with anomalous grain boundaries. The as-cast microstructure consists of a completely cellular array with different cell sizes.

*corresponding author; e-mail: bakourrachda@yahoo.fr

The Pb-rich cellular matrix is represented by light regions and the grain boundaries are represented by dark lines.

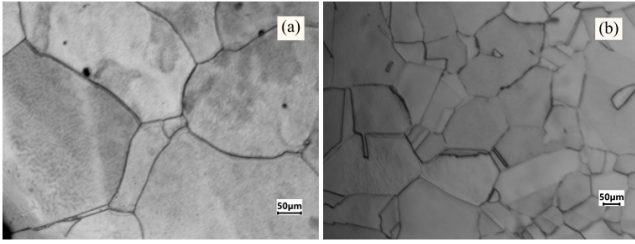


Fig. 1. Typical cellular morphologies of the cross sections of the castings of (a) Pb-1 wt.% Sn and (b) Pb-1 wt.% Sb alloys.

It is clear that Pb-1 wt.% Sn alloy Fig. 1a develops a microstructure with a larger grain size than that in the case of Pb-1 wt.% Sb, Fig. 1b. The average grain size is 200–250 μm for Pb-1 wt.% Sn and 120–160 μm for Pb-1 wt.% Sb.

3.2. Electrochemical corrosion tests

The results from the potentiodynamic polarization curves exhibiting the current densities and corrosion potentials of Pb-1 wt.% Sn and Pb-1 wt.% Sb alloys in 0.5 M H_2SO_4 solution at 25°C are shown in Fig. 2.

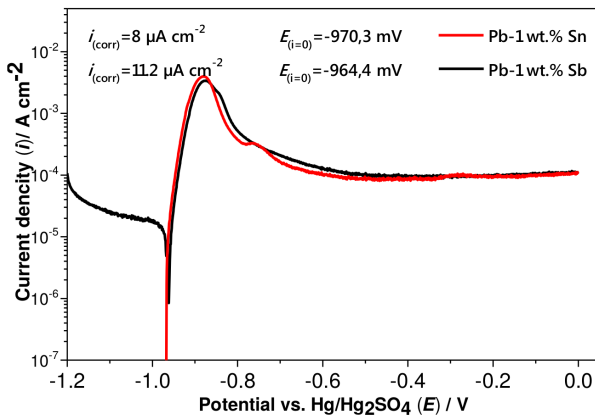


Fig. 2. Potentiodynamic polarization curves for Pb-1 wt.% Sn and Pb-1 wt.% Sb alloys obtained by air casting. The curves were measured in 0.5 M H_2SO_4 solution at 25°C.

The current densities and corrosion potentials for both alloys are reported in Fig. 2. For both alloys, the corrosion potential is almost constant: about -967 ± 3 mV. From the curves we can see that the corrosion current density depends on the nature of the alloying element. Pb-1 wt.% Sn exhibits small corrosion current density ($8 \mu\text{A cm}^{-2}$) in comparison with that for Pb-1 wt.% Sb ($11.2 \mu\text{A cm}^{-2}$). This means that Sn at level of 1 wt.% exhibits good electrochemical corrosion resistance.

3.3. EIS and equivalent circuit analysis

Experimental Nyquist diagrams for Pb-1 wt.% Sn and Pb-1 wt.% Sb measured in 0.5 M aqueous solution of H_2SO_4 at 25°C are given in Fig. 3.

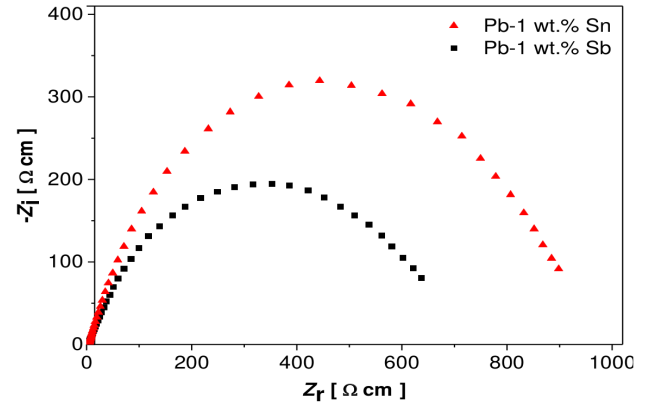


Fig. 3. Nyquist diagrams of the experimental results for Pb-1 wt.% Sn and Pb-1 wt.% Sb in the 0.5 M H_2SO_4 solution at 25°C.

Nyquist plots show that the diameter of the capacitive semi-circle for Pb-1 wt.% Sn is higher than that of Pb-1 wt.% Sb which means that tin provides a better corrosion resistance of the alloy than the antimony.

Figure 4 depicts the Bode and Bode-phase diagrams representing the phase angle θ and modulus of impedance $|Z|$ as functions of frequency.

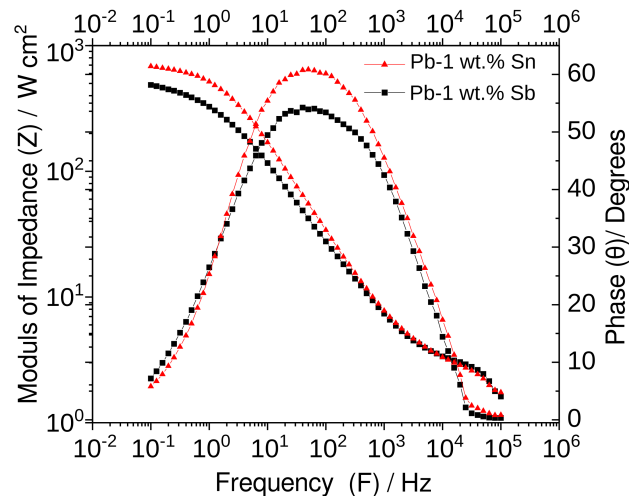


Fig. 4. Experimental EIS diagrams (Bode and Bode-phase) of Pb-1 wt.% Sn and Pb-1 wt.% Sb in the 0.5 M H_2SO_4 solution at 25°C.

The maximum moduli of impedance $|Z|$ of Pb-1 wt.% Sn and Pb-1 wt.% Sb alloys are 684 and 486.7 Ωcm^2 , respectively at 0.1 Hz. Considering the Bode-phase diagrams, the maximum phase angles θ_{max} of about 60.84° at the frequency of 50 Hz and 54.24° at 40 Hz are observed for the Pb-1 wt.% Sn and Pb-1 wt.% Sb alloys, respectively.

These experimental impedance parameters give a clear indication that the Pb-1 wt.% Sn alloy exhibits a better electrochemical behavior when compared to the results corresponding to Pb-1 wt.% Sb.

An equivalent circuit has also been proposed for fitting the experimental data (shown in Fig. 5).

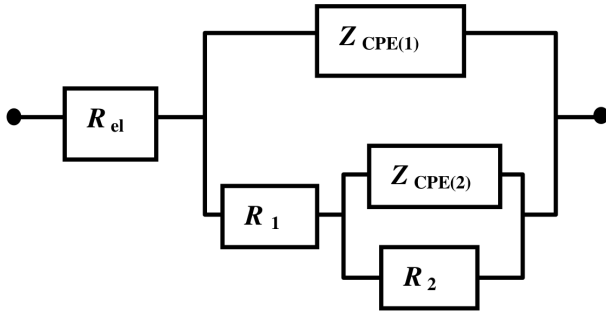


Fig. 5. The proposed equivalent circuit for impedance parameters.

The impedance parameters obtained using the ZView[®] software for Pb-1 wt.% Sn and Pb-1 wt.% Sb alloys are shown in Table I. In the circuit, R_{el} denotes the electrolyte resistance which in the Bode plot is expressed in a high frequency limit ($F > 1$ kHz), R_1 is the charge transfer resistance and R_2 ($F < 0.1$ Hz) stands for the polarization resistance caused by the participation of adsorbed intermediates. $Z_{CPE(1)}$ and $Z_{CPE(2)}$ denote the double-layer capacitance and the capacitance associated with the polarization resistance R_2 .

TABLE I

Impedance parameters obtained using ZView software by fitting the experimental results for Pb-1 wt.% Sn and Pb-1 wt.% Sb alloy samples in the 0.5 M H₂SO₄ solution at 25 °C.

Parameters	Pb-1 wt.% Sn	Pb-1 wt.% Sb
R_{el} [$\Omega \text{ cm}^2$]	2.856	2.881
$Z_{CPE(1)}$ [F cm^{-2}]	61.08×10^{-6}	23.6×10^{-6}
n_1	0.867	0.9579
R_1 [$\Omega \text{ cm}^2$]	10.19	6.034
$Z_{CPE(2)}$ [F cm^{-2}]	0.766×10^{-3}	0.5485×10^{-3}
n_2	0.7032	0.6303
R_2 [$\Omega \text{ cm}^2$]	702.2	185.3
X^2	19.87×10^{-3}	16.31×10^{-3}

Parameters n_1 and n_2 are correlated with the phase angle, varying between 0 and 1. A constant-phase element representing the shift from an ideal capacitor was used for simplicity instead of the capacitance itself. The impedance of a phase element is defined as $Z_{CPE} = 1/[C(j\omega)^n]$ [6–10], where C is the capacitance, j is the electric current, ω is the frequency and $0 \leq n \leq 1$. The value of n seems to be associated with the non-uniform distribution of current as a result of surface roughness and defects.

In Table I it can be observed that $Z_{CPE(1)}$ and $Z_{CPE(2)}$ for coarse cellular spacing are higher than the corresponding values for fine spacing. These capacitances are also associated with the lowest resistances of R_1 and R_2 , which indicate that the coarse cellular array has a better electrochemical corrosion resistance than the fine cellular structure.

4. Conclusions

From the obtained results, we can conclude that the microstructure is an important parameter which controls the corrosion process of alloys used in the lead-acid batteries. Tin added to lead at a level of 1 wt.% exhibits a rather better corrosion resistance than 1 wt.% of Sb.

References

- [1] R.D. Prengaman, *J. Power Sources* **95**, 224 (2001).
- [2] R.D. Prengaman, *J. Power Sources* **158**, 1110 (2006).
- [3] B. Rezaei, S. Damiri, *J. Solid State Electrochem.* **9**, 590 (2005).
- [4] M. Shiota, T. Kameda, K. Matsui, N. Hirai, T. Tanaka, *J. Power Sources* **144**, 358 (2005).
- [5] W.R. Osorio, C.S.C. Aoki, A. Garcia, *J. Power Sources* **185**, 1471 (2008).
- [6] G. Song, A. Atrens, M. Dargusch, *Corros. Sci.* **41**, 249 (1998).
- [7] L. Yu, G.L. Ding, J. Reye, S.N. Tewari, S.N. Ojha, *Metall. Mater. Trans. A* **30**, 2463 (1999).
- [8] D. Pavlov, M. Bojinov, T. Laitinen, G. Sundholm, *Electrochim. Acta* **36**, 2087 (1991).
- [9] W.X. Guo, D. Shu, H.Y. Chen, A.J. Li, H. Wang, G.M. Xiao, C.L. Dou, S.G. Peng, W.W. Wei, W. Zhang, H.W. Zhou, S. Chen, *J. Alloys Compd.* **475**, 102 (2009).
- [10] W.R. Osório, C.M.A. Freire, A. Garcia, *J. Mater. Sci.* **40**, 4493 (2005).